

Synthesis of $\text{YVO}_4\text{:Eu}^{3+}/\text{YBO}_3$ Heteronanostructures with Enhanced Photoluminescence Properties

Hongliang Zhu · Haihua Hu · Zhengkai Wang ·
Diantai Zuo

Received: 6 January 2009 / Accepted: 14 May 2009 / Published online: 29 May 2009
© to the authors 2009

Abstract Novel $\text{YVO}_4\text{:Eu}^{3+}/\text{YBO}_3$ core/shell heteronanostructures with different shell ratios (SRs) were successfully prepared by a facile two-step method. X-ray diffraction, transmission electron microscopy and X-ray photoelectron spectroscopy were used to characterize the heteronanostructures. Photoluminescence (PL) study reveals that PL efficiency of the $\text{YVO}_4\text{:Eu}^{3+}$ nanocrystals (cores) can be improved by the growth of YBO_3 nanocoatings onto the cores to form the $\text{YVO}_4\text{:Eu}^{3+}/\text{YBO}_3$ core/shell heteronanostructures. Furthermore, shell ratio plays a critical role in their PL efficiency. The heteronanostructures (SR = 1/7) exhibit the highest PL efficiency; its PL intensity of the $^5\text{D}_0\text{--}^7\text{F}_2$ emission at 620 nm is 27% higher than that of the $\text{YVO}_4\text{:Eu}^{3+}$ nanocrystals under the same conditions.

Keywords Core/shell heteronanostructures · Nanophosphors · Photoluminescence · Yttrium vanadate · Yttrium borate

Introduction

Rare-earth (RE)-doped phosphors have a broad range of applications in cathode ray tubes (CRTs), plasma display panels (PDPs), field emission displays (FEDs), X-ray detectors, fluorescent lamps and so on [1–3]. In recent years,

RE-doped nanophosphors have received a great deal of research attention due to the unique applications in higher-resolution displays, drug delivery system and biological fluorescence labeling [4–8]. Furthermore, fluorescent lamps made from small-sized phosphors always have high-packing density and low loading [9]. RE-doped nanophosphors are expected to have high brightness and luminescence quantum yield for practical applications. Unfortunately, high specific surface area and surface defects of the nanophosphors always result in serious surface recombination, which is a pathway for nonradiative relaxation [10]. Consequently, RE-doped nanophosphors have lower luminescence efficiency compared to their corresponding bulk powder phosphors [11, 12]. More attention should be paid to improve the luminescence efficiency of RE-doped nanophosphors.

During the past decade, core/shell heteronanostructures have been widely investigated to obtain better properties [13, 14]. Luminescence efficiency of RE-doped nanophosphors can be improved by forming core/shell heteronanostructures, because surface defects and surface recombination of the nanophosphors (cores) are greatly reduced by the nanocoatings (shells) [11, 15]. Among RE-doped phosphors, europium ions-doped yttrium orthovanadate ($\text{YVO}_4\text{:Eu}^{3+}$) is an important red phosphor, which has been commercially used in CRTs, high-pressure mercury lamps and color television due to its excellent luminescence properties [2, 3]. Many literatures have reported the preparation and luminescence properties of $\text{YVO}_4\text{:Eu}^{3+}$ nanophosphors [16–18], but few measures have been taken to improve their luminescence efficiency. In this paper, we propose novel $\text{YVO}_4\text{:Eu}^{3+}/\text{YBO}_3$ core/shell heteronanostructures that exhibit enhanced photoluminescence efficiency. Compared to the reported heteronanostructures of $\text{YVO}_4\text{:Eu}^{3+}$ such as $\text{Y}_2\text{O}_3\text{:Eu}^{3+}@/\text{SiO}_2@/\text{YVO}_4\text{:Eu}^{3+}$, $\text{SiO}_2@/\text{YVO}_4\text{:Eu}^{3+}$ and $\text{YV}_{0.7}\text{P}_{0.3}\text{O}_4\text{:Eu}^{3+},\text{Bi}^{3+}@/\text{SiO}_2$ [19–21], yttrium borate

H. Zhu (✉) · Z. Wang · D. Zuo
Center of Materials Engineering, Zhejiang Sci-Tech University,
Xiasha University Town, 310018 Hangzhou, China
e-mail: zhuhl@zstu.edu.cn

H. Hu
Zhejiang University City College, 310015 Hangzhou, China

(YBO₃), is used as shell material in this new heteronanostructures. YBO₃ has excellent properties such as high VUV transparency, high stability, low synthesis temperature and exceptional optical damage threshold [22, 23], so the new core/shell heteronanostructures proposed here may have promising applications in the fields of display, lighting and bio-nanotechnology.

Experimental

The YVO₄:Eu³⁺/YBO₃ core/shell heteronanostructures were prepared by a facile two-step method. The YVO₄:Eu³⁺ nanocrystals (cores) doped with 5 mol% europium were prepared by hydrothermal method. The YBO₃ nanocoatings (shells) were grown onto the cores by the sol–gel method reported in our previous literature [22]. The shell ratio (SR) is molar percentage of the shell material (YBO₃) in the core/shell heteronanostructures. In this study, different shell ratios such as 1/9, 1/8, 1/7, 1/5, 1/3, 1/2 and 2/3 were adopted, so a total of seven heteronanostructures were prepared.

Preparation of YVO₄:Eu³⁺ Nanocrystals

To 130 mL of deionized water, 30.4 mL of Y(NO₃)₃ solution (0.15 mol/L), 1.6 mL of Eu(NO₃)₃ solution (0.15 mol/L) and 0.758 g of NaVO₃·2H₂O were added under vigorous magnetic stirring for 30 min. The pH value of the solution was adjusted to 9.5 using ammonia under stirring. Then, the above solution was transferred into a Teflon-lined stainless steel autoclave (capacity 200 mL) and sealed. The autoclave was heated at 200 °C for 16 h and cooled naturally to room temperature. Finally, the YVO₄:Eu³⁺ nanocrystals were collected by centrifugation.

Preparation of Sol–Gel Solution

To 100 mL of water–ethanol solution (the volume ratio is 1:4) 3.83 g of Y(NO₃)₃·6H₂O and 0.68 g of H₃BO₃ (~10 mol% of excess) were added under stirring. To the above solution, 6.30 g of citric acid (CA) and 12.00 g of PEG 6000 (the molar ratio of Y(NO₃)₃, CA, and PEG was 5:15:1) were added. Herein, CA and PEG were used as the chelating and cross-linking reagents respectively. The above solution was stirred for 5 h and subsequently aged for 24 h. Finally, highly transparent sol–gel solution with yttrium concentration of 0.1 mol/L was obtained.

Preparation of YVO₄:Eu³⁺/YBO₃ Heteronanostructures

Herein, we take the heteronanostructures (SR = 1/7) as an example to present their detailed procedures. The YVO₄:Eu³⁺ nanocrystals (4.56 mmol) obtained in the first

step were heated to 120 °C in a petri dish. Then, 6.51 mL of the sol–gel solution was slowly dropped onto the heated YVO₄:Eu³⁺ nanocrystals. The obtained sample was annealed at 700 °C in air for 2 h with a heating rate of 1 °C/min. The furnace was cooled to room temperature naturally and the white YVO₄:Eu³⁺/YBO₃ heteronanostructures (SR = 1/7) were obtained.

In this paper the YVO₄:Eu³⁺ (5 mol% Eu) nanocrystals obtained in the first step are called “the original sample”. To avoid the influence of annealing on the photoluminescence property, the original sample was also annealed at 700 °C for 2 h under the same conditions. The annealed original sample is denoted as “YVO₄:Eu³⁺/YBO₃ core/shell heteronanostructures (SR = 0)”. In addition, YBO₃ powder was prepared by the above-mentioned sol–gel approach, for comparison.

Characterization and Photoluminescence Property

Phase identification of the products was carried out using a Thermo ARL X'TRA X-ray diffractometer (XRD) with Cu K α radiation (λ = 1.54178 Å). Morphology observation of the original sample was observed using a JEOL JEM 200 CX transmission electron microscope (TEM). In addition, a Philips CM200 high-resolution transmission electron microscope (HRTEM) with an accelerating voltage of 200 kV was also employed to investigate the morphology and structure of the core/shell heteronanostructures (SR = 1/2). X-ray photoelectron spectroscopy (XPS) measurement was performed on a X-ray photoelectron spectrometer (Model Axis Ultra DLD, Kratos Corp., UK) with a standard MgK α (1,256.6 eV) X-ray source operating at 150 W. All binding energies were referenced to the C 1 s peak at 284.6 eV of the surface adventitious carbon. Photoluminescence (PL) excitation and emission spectra of all the powder products were obtained on a Hitachi fluorescence spectrophotometer (Model F-4600, Hitachi Corporation, Japan) under the same conditions.

Results and Discussion

All as-synthesized products were characterized by XRD, and their data were analyzed by a Thermo ARL WinXRD software package. Figure 1 shows XRD patterns of the original sample (the YVO₄ nanocrystals obtained in the first step), typical core/shell heteronanostructures and YBO₃ powder. As shown in Fig. 1a, all XRD peaks are in good agreement with the values of YVO₄ (JCPDS no. 72–0274) confirming that the core material was YVO₄:Eu³⁺. Likewise, the XRD pattern of the YBO₃ prepared by the sol–gel method is in good agreement with the standard card of YBO₃ (JCPDS no. 16-0277). Therefore, pure YBO₃ can

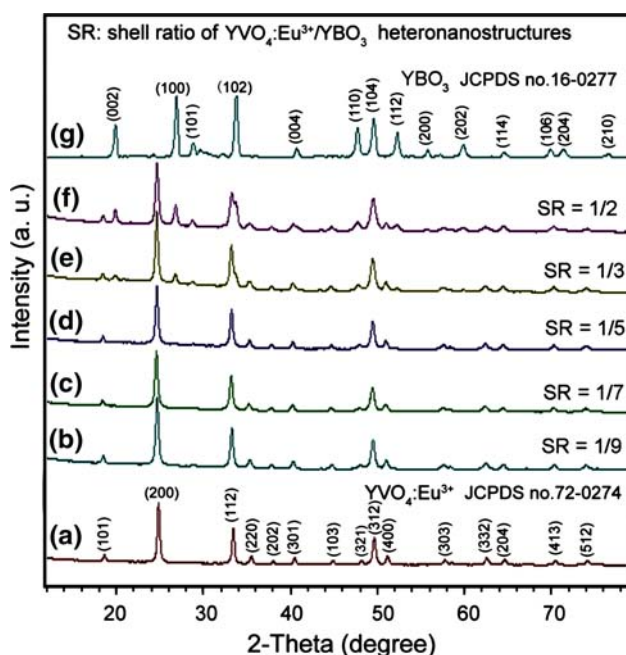


Fig. 1 XRD patterns of the typical products. *a* The $\text{YVO}_4:\text{Eu}^{3+}$ nanocrystals. *b–f* The $\text{YVO}_4:\text{Eu}^{3+}/\text{YBO}_3$ heteronanostructures. *g* The YBO_3 powder

be successfully obtained by the sol–gel approach. As shown in Fig. 1b–f, the $\text{YVO}_4:\text{Eu}^{3+}/\text{YBO}_3$ core/shell heteronanostructures exhibit two series of XRD patterns, namely, those of YVO_4 and YBO_3 . In addition, the intensities of the peaks of YBO_3 increase with the shell ratio. Figure 2 shows enlarged XRD patterns of some typical products, which clearly demonstrate that the XRD peaks of both YVO_4 and YBO_3 could be found in the heteronanostructures. Therefore, the heteronanostructures are composed of the $\text{YVO}_4:\text{Eu}^{3+}$ and YBO_3 .

Transmission electron microscope images of the original sample (the $\text{YVO}_4:\text{Eu}^{3+}$ nanocrystals obtained in the first step) and $\text{YVO}_4:\text{Eu}^{3+}/\text{YBO}_3$ core/shell heteronanostructures ($\text{SR} = 1/2$) are shown in Fig. 3. Figure 3a reveals that the original sample used as the core is nanocrystals. The inset of Fig. 3a clearly shows that the $\text{YVO}_4:\text{Eu}^{3+}$ nanocrystals are around 20 nm in diameter. The core/shell heteronanostructures were obtained by sol–gel growth of YBO_3 nanocoatings onto the $\text{YVO}_4:\text{Eu}^{3+}$ nanocrystals, so their particle sizes were larger than that of the $\text{YVO}_4:\text{Eu}^{3+}$ nanocrystals. Figure 3b shows TEM image of the core/shell heteronanostructures ($\text{SR} = 1/2$). As shown in Fig. 3b, the heteronanostructures have a similar morphology to the original sample, while the average particle size of the heteronanostructures is approximately twice larger than the original $\text{YVO}_4:\text{Eu}^{3+}$ nanocrystals. This phenomenon indirectly verifies that the YBO_3 nanocoatings have been grown onto the $\text{YVO}_4:\text{Eu}^{3+}$ nanocrystals by the

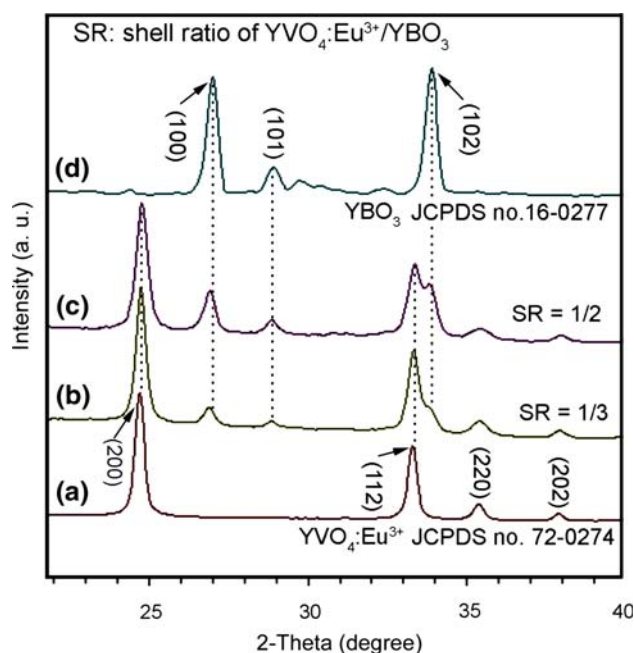


Fig. 2 Enlarged XRD patterns in range of 20–40°. *a* The $\text{YVO}_4:\text{Eu}^{3+}$ nanocrystals. *b* The $\text{YVO}_4:\text{Eu}^{3+}/\text{YBO}_3$ ($\text{SR} = 1/3$). *c* The $\text{YVO}_4:\text{Eu}^{3+}/\text{YBO}_3$ ($\text{SR} = 1/2$). *d* The YBO_3 powder

sol–gel process. Figure 3c is HRTEM image of a single particle of the heteronanostructures ($\text{SR} = 1/2$). Interestingly, two lattice fringes of different spacing appear in a single nanoparticle. The lattice fringes with a d-spacing of about 0.473 nm are found at the center of the particle, while the lattice fringe spacing is 0.308 nm in the peripheral zones of the particle. The two different types of the lattice fringes correspond well to the {101} planes of YVO_4 (JCPDS no. 72–0274) and the {101} planes of YBO_3 (JCPDS no. 16–0277), respectively. Therefore, $\text{YVO}_4:\text{Eu}^{3+}/\text{YBO}_3$ core/shell heteronanostructures were formed by the two-step process.

X-ray photoelectron spectroscopy is the most commonly used technique for investigating the elemental composition of surface layers 1–5 nm in depth. Herein, XPS was used to further determine the formation of the $\text{YVO}_4:\text{Eu}^{3+}/\text{YBO}_3$ core/shell heteronanostructures. If the $\text{YVO}_4:\text{Eu}^{3+}$ cores were effectively coated with the shell material (YBO_3), the XPS peak intensities of the core material ($\text{YVO}_4:\text{Eu}^{3+}$) would be very low. In other words, whether or not the product was the $\text{YVO}_4:\text{Eu}^{3+}/\text{YBO}_3$ core/shell heteronanostructures could be determined by the XPS bands of vanadium. Figure 4 shows XPS spectra of the $\text{YVO}_4:\text{Eu}^{3+}/\text{YBO}_3$ heteronanostructures ($\text{SR} = 1/2$), $\text{YVO}_4:\text{Eu}^{3+}$ nanocrystals and YBO_3 powder. XPS spectra in the range of 135–210 eV (Fig. 4a) reveals that B 1 s bands at 191.0 eV are clearly found in the YBO_3 powder and the $\text{YVO}_4:\text{Eu}^{3+}/\text{YBO}_3$ heteronanostructures [24], while not detected in the $\text{YVO}_4:\text{Eu}^{3+}$ nanocrystals. The strongest

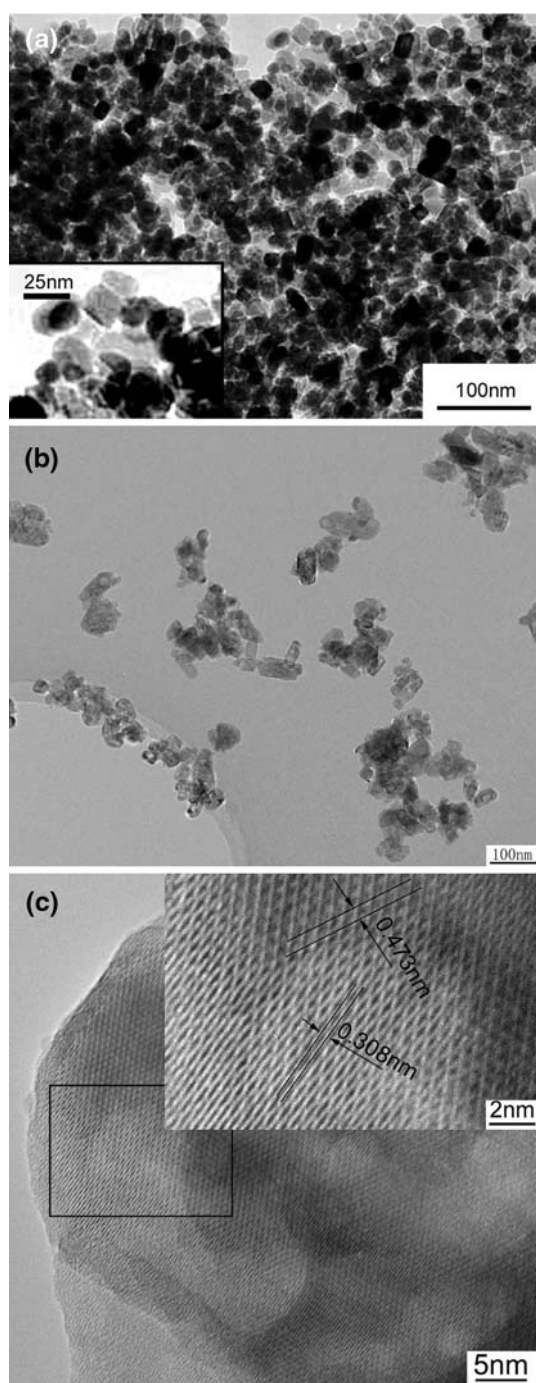


Fig. 3 TEM and HRTEM images of the typical products. **a** TEM image of the $\text{YVO}_4:\text{Eu}^{3+}$ nanocrystals. **b** TEM image of the $\text{YVO}_4:\text{Eu}^{3+}/\text{YBO}_3$ (SR = 1/2). **c** HRTEM image of the $\text{YVO}_4:\text{Eu}^{3+}/\text{YBO}_3$ (SR = 1/2). The insets are their respective magnified images

XPS band of vanadium is located at 515.6 eV, which is assigned to V 2p [25]. As shown in Fig. 4b, the V 2p band of the $\text{YVO}_4:\text{Eu}^{3+}$ nanocrystals is very strong, while that of the $\text{YVO}_4:\text{Eu}^{3+}/\text{YBO}_3$ heteronanostructures (SR = 1/2) is much lower. This is because the $\text{YVO}_4:\text{Eu}^{3+}$ cores have

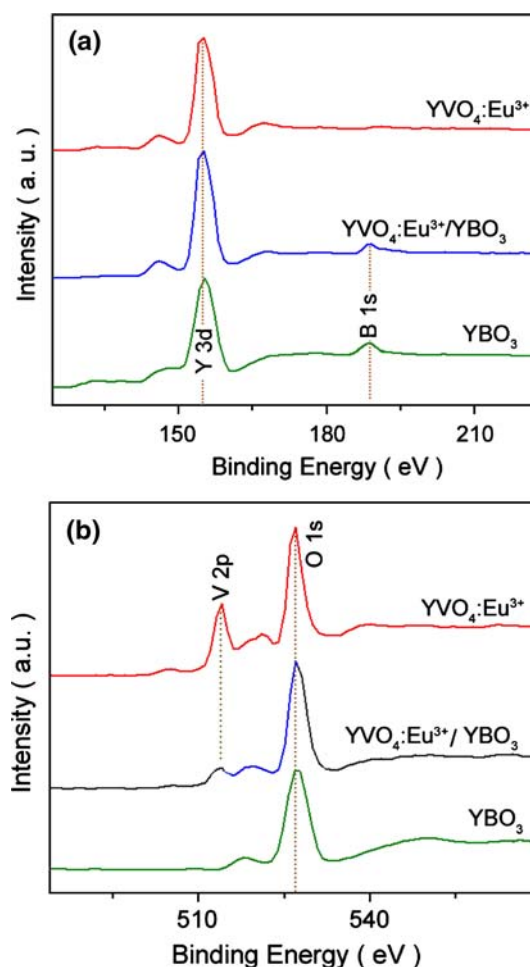


Fig. 4 XPS spectra of the $\text{YVO}_4:\text{Eu}^{3+}/\text{YBO}_3$ heteronanostructures (SR = 1/2) $\text{YVO}_4:\text{Eu}^{3+}$ nanocrystals and YBO_3 powder in range of **a** 135–210 eV and **b** 495–555 eV

been coated with YBO_3 nanocoatings and no enough V 2p XPS signal from the cores was generated by X-ray source.

High photoluminescence (PL) efficiency is important for practical applications of $\text{YVO}_4:\text{Eu}^{3+}$ nanophosphors. The $\text{YVO}_4:\text{Eu}^{3+}/\text{YBO}_3$ core/shell heteronanostructures reported here are expected to exhibit enhanced PL efficiency under the same conditions. All PL excitation and emission spectra of the samples were measured in powder form using the same measurement parameters, so their respective PL emission intensity can relatively represent their PL efficiency. Figure 5a, b shows PL excitation and emission spectra of the $\text{YVO}_4:\text{Eu}^{3+}/\text{YBO}_3$ core/shell heteronanostructures and original $\text{YVO}_4:\text{Eu}^{3+}$ nanocrystals and annealed $\text{YVO}_4:\text{Eu}^{3+}$ nanocrystals respectively. As shown in the excitation spectra (Fig. 5a), the heteronanostructures and $\text{YVO}_4:\text{Eu}^{3+}$ nanocrystals exhibit a similar broad excitation band in the range of 200–360 nm with a maximum value at 320 nm, which is ascribed to a charge transfer from the oxygen ligands to the central vanadium

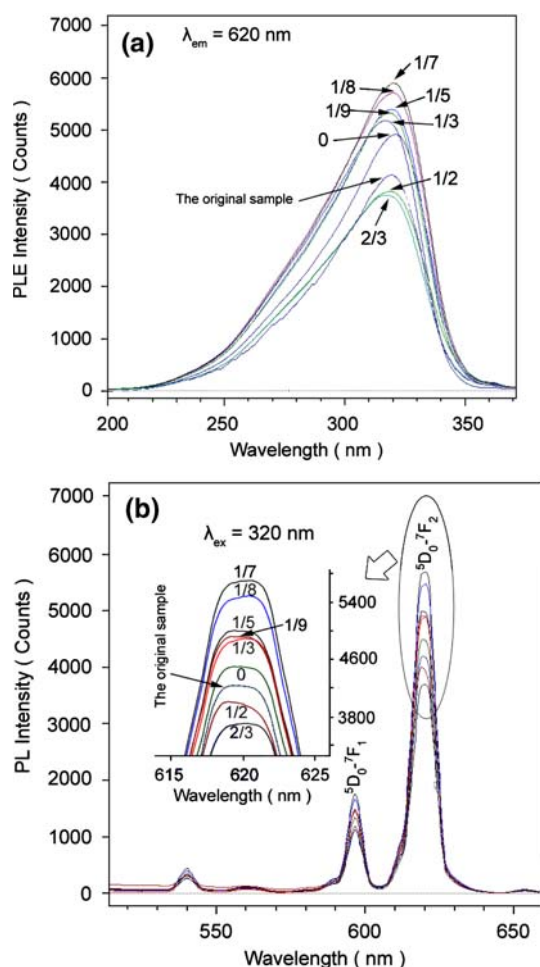


Fig. 5 Photoluminescence (a) excitation and (b) emission spectra of the $\text{YVO}_4:\text{Eu}^{3+}/\text{YBO}_3$ core/shell heteronanostructures

atom inside the VO_4^{3-} ion [5, 26]. As shown in Fig. 5b, both the $\text{YVO}_4:\text{Eu}^{3+}$ nanocrystals and the heteronanostructures show two well-known PL emission bands in the range of 550–650 nm. The two emission bands at 596 nm and 620 nm are assigned to the magnetic-dipole transition $^5\text{D}_0-^7\text{F}_1$ of Eu^{3+} (596 nm) and the forced electric-dipole transition $^5\text{D}_0-^7\text{F}_2$ of Eu^{3+} (620 nm), respectively [27]. Herein, the $^5\text{D}_0-^7\text{F}_2$ emission at 620 nm (red emission) is selected as a criterion to determine their relative PL efficiency. The annealed $\text{YVO}_4:\text{Eu}^{3+}$ nanocrystals exhibit a little stronger PL emission than the original sample, because the crystallinity of the nanocrystals was improved by the annealing process. However, the influence of annealing on the photoluminescence properties can be avoided by comparison between the annealed sample and the heteronanostructures. Figure 5 reveals that all the heteronanostructures except for those with the shell ratios of 1/2 and 2/3 exhibit much stronger photoluminescence than the annealed $\text{YVO}_4:\text{Eu}^{3+}$ nanocrystals under the same conditions. Furthermore, the shell ratio plays a critical role

in the PL efficiency of the heteronanostructures. When $\text{SR} = 1/7$, the heteronanostructures exhibit the highest PL efficiency, whose photoluminescence intensity of the $^5\text{D}_0-^7\text{F}_2$ emission is 27% higher than that of the annealed $\text{YVO}_4:\text{Eu}^{3+}$ nanocrystals. Therefore, PL efficiency of $\text{YVO}_4:\text{Eu}^{3+}$ nanophosphor can be improved by forming $\text{YVO}_4:\text{Eu}^{3+}/\text{YBO}_3$ core/shell heteronanostructures.

Nanostructured materials have a high surface area-to-volume ratio, and this characteristic inevitably results in high surface defects density and serious surface recombination. Therefore, RE-doped nanophosphors suffer more serious nonradiative relaxation than corresponding bulk power phosphors. Consequently, RE-doped nanophosphors always have lower luminescence efficiency. In this paper, the nonradiative decay of the $\text{YVO}_4:\text{Eu}^{3+}$ nanocrystals was greatly reduced by the YBO_3 nanocoating on the $\text{YVO}_4:\text{Eu}^{3+}$ nanocrystals, so PL emission of the heteronanostructures was enhanced. YBO_3 has excellent properties such as high VUV transparency, high stability, low synthesis temperature and exceptional optical damage threshold [22, 23]; so, it is an ideal shell material for composite phosphors with core/shell heterostructures. The YBO_3 shell ratio is a critical factor in photoluminescence enhancement of the heteronanostructures. Figure 6 shows the plot of change of PL intensity of the $^5\text{D}_0-^7\text{F}_2$ emission at 620 nm with the shell ratio. The change exhibits a parabola-like curve that reaches the peak at $\text{SR} = 1/7$. When $\text{SR} < 1/7$, PL intensity increases with increasing SR. This is because the surface recombination, surface defects density and surface state density of $\text{YVO}_4:\text{Eu}^{3+}$ nanocrystals decrease with increasing the YBO_3 coating. When $\text{SR} = 1/7$, the surface recombination, surface defects density and surface state density have been decreased to the maximum level, so

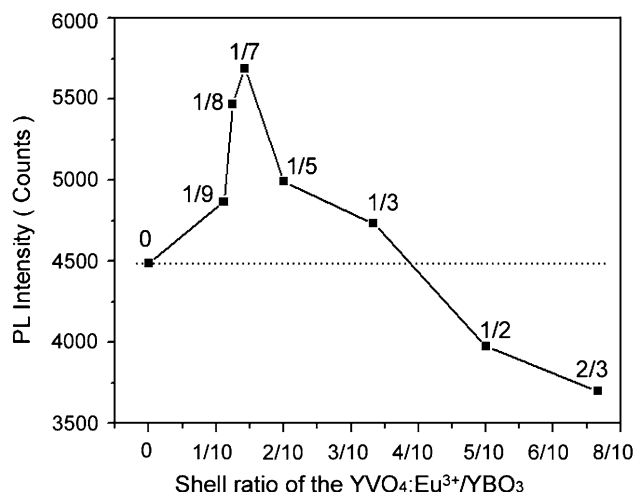


Fig. 6 Change of PL intensity of the $^5\text{D}_0-^7\text{F}_2$ emission of the $\text{YVO}_4:\text{Eu}^{3+}/\text{YBO}_3$ core/shell heteronanostructures with shell ratio

the strongest PL emission was obtained. When $SR > 1/7$, PL intensity decreases with increasing molar percentage of the nonluminescent shell material (YBO_3).

Conclusions

$YVO_4:Eu^{3+}/YBO_3$ core/shell heteronanostructures with different shell ratios (SRs) were successfully prepared by sol–gel growth of YBO_3 nanocoating onto the $YVO_4:Eu^{3+}$ nanocrystals. Characterizations by means of XRD, TEM and XPS confirmed the formation of the $YVO_4:Eu^{3+}/YBO_3$ core/shell heteronanostructures. The heteronanostructures exhibited much stronger photoluminescence (PL) than the $YVO_4:Eu^{3+}$ nanocrystals under the same conditions. The shell ratio is a critical factor in PL enhancement of the heteronanostructures. When $SR = 1/7$, the heteronanostructures exhibited the highest PL efficiency, whose PL intensity ($^5D_0-^7F_2$ emission) was 27% higher than that of the $YVO_4:Eu^{3+}$ nanocrystals. YBO_3 is an ideal shell material for composite phosphors with core/shell heterostructures due to its high VUV transparency, high stability, low synthesis temperature and exceptional optical damage threshold.

Acknowledgments This work was supported by the Teaching and Research Award Program for Outstanding Young Teachers in Higher Education Institutions of Zhejiang Province. Authors also thank financial supports from the Doctoral Science Foundation of Zhejiang Sci-Tech University (no. 0803611-Y).

References

1. C. Feldmann, T. Jüstel, C.R. Ronda, P.J. Schmidt, *Adv. Funct. Mater.* **13**, 511 (2003). doi:[10.1002/adfm.200301005](https://doi.org/10.1002/adfm.200301005)
2. T. Jüstel, H. Nikol, C. Ronda, *Angew. Chem. Int. Ed.* **37**, 3084 (1998). doi:[10.1002/\(SICI\)1521-3773\(19981204\)37:22<3084::AID-ANIE3084>3.0.CO;2-W](https://doi.org/10.1002/(SICI)1521-3773(19981204)37:22<3084::AID-ANIE3084>3.0.CO;2-W)
3. G. Blasse, B.C. Grabmeier, *Luminescent materials* (Springer, Berlin, 1994)
4. H. Chander, *Mater. Sci. Eng. Rep.* **49**, 113 (2005). doi:[10.1016/j.mser.2005.06.001](https://doi.org/10.1016/j.mser.2005.06.001)
5. H. Zhu, H. Yang, D. Jin, Z. Wang, X. Gu, X. Yao, K. Yao, J. *Nanopart. Res.* **10**, 1149 (2008). doi:[10.1007/s11051-007-9339-y](https://doi.org/10.1007/s11051-007-9339-y)
6. P. Yang, Z. Quan, L. Lu, S. Huang, J. Lin, H. Fu, *Nanotechnology* **18**, 235703 (2007). doi:[10.1088/0957-4484/18/23/235703](https://doi.org/10.1088/0957-4484/18/23/235703)
7. D. Giaume, M. Poggi, D. Casanova, G. Mialon, K. Lahliil, A. Alexandrou, T. Gacoin, J.-P. Boilot, *Langmuir* **24**, 11018 (2008). doi:[10.1021/la8015468](https://doi.org/10.1021/la8015468)
8. S. Ben-David Makhluף, R. Arnon, C.R. Patra, D. Mukhopadhyay, A. Gedanken, P. Mukherjee, H. Breitbart, *J. Phys. Chem. C* **112**, 12801 (2008). doi:[10.1021/jp804012b](https://doi.org/10.1021/jp804012b)
9. R.P. Rao, *J. Lumin.* **113**, 271 (2005). doi:[10.1016/j.jlumin.2004.10.018](https://doi.org/10.1016/j.jlumin.2004.10.018)
10. B.L. Abrams, P.H. Holloway, *Chem. Rev.* **104**, 5783 (2004). doi:[10.1021/cr020351r](https://doi.org/10.1021/cr020351r)
11. W. Bu, Z. Hua, H. Chen, J. Shi, *J. Phys. Chem. B* **109**, 14461 (2005). doi:[10.1021/jp052486h](https://doi.org/10.1021/jp052486h)
12. S. Lu, A. Madhukar, *Nano. Lett.* **7**, 3443 (2007). doi:[10.1021/nl0719731](https://doi.org/10.1021/nl0719731)
13. W. Luan, H. Yang, N. Fan, S.T. Tu, *Nanoscale Res. Lett.* **3**, 134 (2008). doi:[10.1007/s11671-008-9125-5](https://doi.org/10.1007/s11671-008-9125-5)
14. C.Q. Zhu, P. Wang, X. Wang, Y. Li, *Nanoscale Res. Lett.* **3**, 213 (2008). doi:[10.1007/s11671-008-9139-z](https://doi.org/10.1007/s11671-008-9139-z)
15. C. Louis, S. Roux, G. Ledoux, C. Dujardin, O. Tillement, B.L. Cheng, P. Perriat, *Chem. Phys. Lett.* **429**, 157 (2006). doi:[10.1016/j.cplett.2006.06.085](https://doi.org/10.1016/j.cplett.2006.06.085)
16. A. Huignard, V. Buissette, G. Laurent, T. Gacoin, J.-P. Boilot, *Chem. Mater.* **14**, 2264 (2002). doi:[10.1021/cm011263a](https://doi.org/10.1021/cm011263a)
17. G. Li, K. Chao, H. Peng, K. Chen, *J. Phys. Chem. C* **112**, 6228 (2008). doi:[10.1021/jp710451r](https://doi.org/10.1021/jp710451r)
18. K. Riwotzki, M. Haase, *J. Phys. Chem. B* **102**, 10129 (1998). doi:[10.1021/jp982293c](https://doi.org/10.1021/jp982293c)
19. M. Chang, S. Tie, *Nanotechnology* **19**, 075711 (2008). doi:[10.1088/0957-4484/19/7/075711](https://doi.org/10.1088/0957-4484/19/7/075711)
20. M. Darbandi, W. Hoheisel, T. Nann, *Nanotechnology* **17**, 4168 (2006). doi:[10.1088/0957-4484/17/16/029](https://doi.org/10.1088/0957-4484/17/16/029)
21. M. Yu, J. Lin, J. Fang, *Chem. Mater.* **17**, 1783 (2005). doi:[10.1021/cm0479537](https://doi.org/10.1021/cm0479537)
22. H. Zhu, L. Zhang, T. Zuo, X. Gu, Z. Wang, L. Zhu, K. Yao, *Appl. Surf. Sci.* **254**, 6362 (2008). doi:[10.1016/j.apsusc.2008.03.183](https://doi.org/10.1016/j.apsusc.2008.03.183)
23. M. Tükia, J. Hölsä, M. Lastusaari, J. Niittykoski, *Opt. Mater.* **27**, 1516 (2005). doi:[10.1016/j.optmat.2005.01.017](https://doi.org/10.1016/j.optmat.2005.01.017)
24. G.D. Khattak, M.A. Salim, L.E. Wenger, A.H. Gilani, *J. Non-Cryst. Solids* **244**, 128 (1999). doi:[10.1016/S0022-3093\(99\)00051-4](https://doi.org/10.1016/S0022-3093(99)00051-4)
25. D. Barreca, L.E. Depero, V. Di Noto, G.A. Rizzi, L. Sangaletti, E. Tondello, *Chem. Mater.* **11**, 255 (1999). doi:[10.1021/cm980725q](https://doi.org/10.1021/cm980725q)
26. Y. Li, G. Hong, *J. Solid. State. Chem.* **178**, 645 (2005). doi:[10.1016/j.jssc.2004.12.018](https://doi.org/10.1016/j.jssc.2004.12.018)
27. H. Zhu, D. Yang, L. Zhu, D. Li, P. Chen, G. Yu, *J. Am. Ceram. Soc.* **90**, 3095 (2007). doi:[10.1111/j.1551-2916.2007.01851.x](https://doi.org/10.1111/j.1551-2916.2007.01851.x)